

Current Confinement Effect on the Performance of Blue Light Micro-LEDs with 10 μm Dimension

Yu-Hsuan Hsu, Yi-Hsin Lin, Ming-Hsien Wu, Hao Chung Kuo, and Ray-Hua Horng*

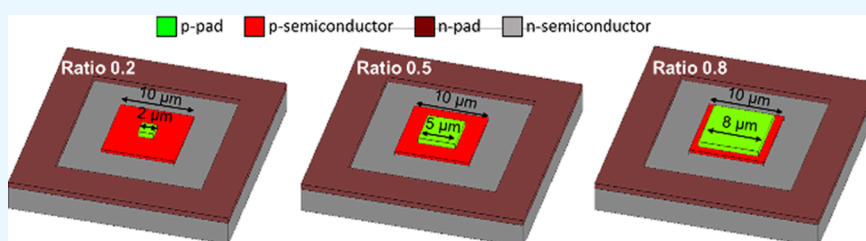
Cite This: *ACS Omega* 2023, 8, 35351–35358

Read Online

ACCESS |

Metrics & More

Article Recommendations



ABSTRACT: The current confinement effect on the micro-LED (μLED) with a 10 μm dimension was simulated using SpeCLED software. In this study, three p-contact sizes were considered: 2 $\mu\text{m} \times 2 \mu\text{m}$, 5 $\mu\text{m} \times 5 \mu\text{m}$, and 8 $\mu\text{m} \times 8 \mu\text{m}$ dimensions for μLED s with a 10 μm dimension. According to the simulation data, the highest external quantum efficiency (EQE) of 13.24% was obtained with a 5 $\mu\text{m} \times 5 \mu\text{m}$ contact size. The simulation data also showed that the μLED s with narrow contact sizes experienced higher operating temperatures due to the current crowding effect. The experimental data revealed a red-shift effect in narrow contact sizes, indicating higher heat generation in those devices. As the contact sizes increased from 2 to 8 μm , the turn-on voltage decreased due to lower equivalent resistance. Additionally, the leakage current increased from 44 pA to 1.6 nA at a reverse voltage of -5 V . The study found that the best performance was achieved with a contact ratio of 0.5, which resulted in the highest EQE at 9.95%. This superior performance can be attributed to the better current confinement of the μLED compared to the μLED with a contact ratio of 0.8, resulting in lower leakage current and improved current spreading when compared to the μLED with a contact ratio of 0.2.

INTRODUCTION

Inorganic light-emitting diodes (LEDs) have the advantage of self-emission compared to commercial liquid crystal displays (LCDs). LEDs offer reduced power consumption, longer lifetime, and greater stability than organic LEDs (OLEDs).^{1–3} The microscale LED chip size, known as μLED , is considered the next-generation display technology, offering high resolution, high contrast ratio, and promising applications.⁴ Particularly in augmented and mixed reality (AR/MR) glasses, these displays require a very high pixel-per-inch (PPI), high brightness with efficient illumination, and contrast ratio in a small active region. To achieve a full-color display, the direct mass transfer of red, green, and blue LED chips to the display has been utilized.^{5–9} However, as the chip size is reduced to a micrometer scale, the mass transfer method becomes challenging to implement. Several potential solutions have been proposed, including the use of a color conversion layer (CCL) and the integration of colloidal quantum dots (QDs) with a monochromatic μLED array. The integration of QDs and μLED arrays demonstrates a high potential for achieving high-resolution full-color displays. Coating QDs on substrates can be achieved through photolithography, transfer printing, and inkjet printing.^{10–14} The smallest RGB subpixel pattern resolutions achieved with these QD fabrications are 14 $\mu\text{m} \times$

14 μm ,¹² 5 $\mu\text{m} \times 39 \mu\text{m}$,¹³ and 50 $\mu\text{m} \times 50 \mu\text{m}$.¹⁴ For these applications, a high-efficiency blue light source with an InGaN/GaN structure is commonly used to excite the material and achieve a full-color display.^{15,16} Researchers have explored various methods to passivate small-sized μLED s, including changing the material of the passivation layer^{17–20} or growing denser films using the ALD process.^{21–24} Passivation of sidewalls using chemical solutions has also been proposed to reduce leakage current in small-sized μLED s.^{25–28} While these methods can improve device performance, they also increase process costs.

In our previous investigation,²⁹ we studied the impact of the indium tin oxide (ITO) contact size on the electrical and optical properties of 40 $\mu\text{m} \times 40 \mu\text{m}$ μLED s. We found that wider contact sizes in these μLED s resulted in a lower turn-on voltage and series resistance. As a result, larger contact sizes exhibited higher emission power and a more uniform emission

Received: July 21, 2023

Accepted: August 30, 2023

Published: September 11, 2023



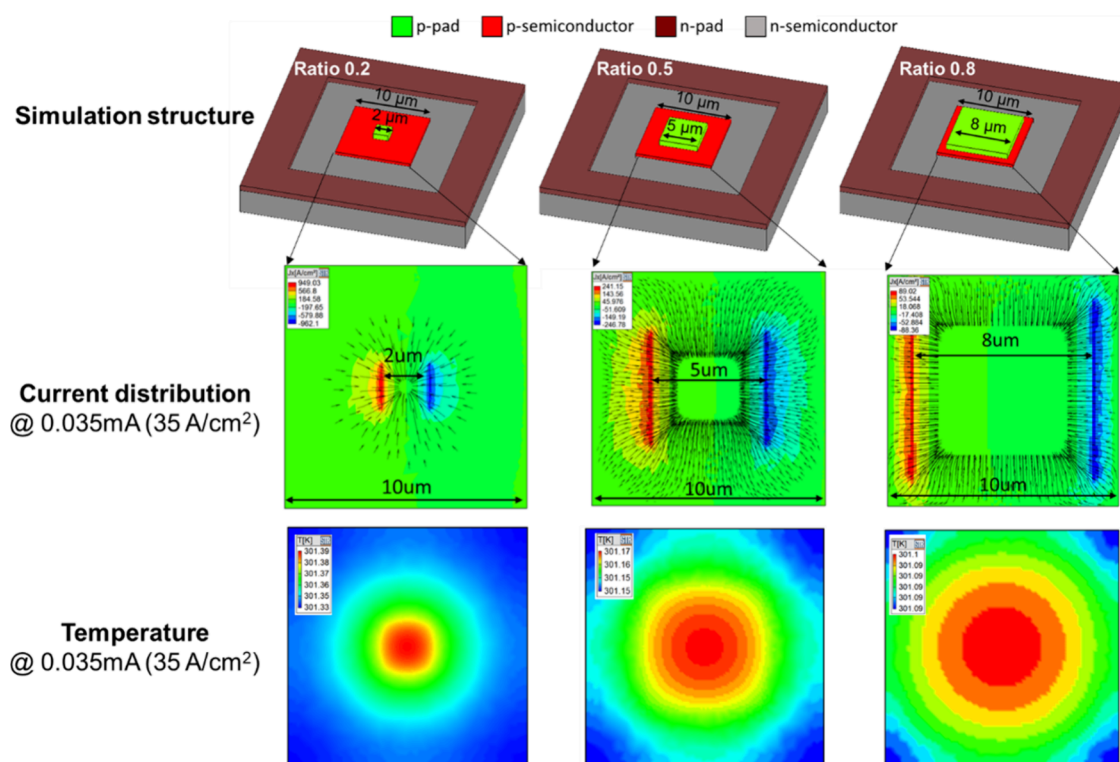


Figure 1. 3D structure of μ LEDs, lateral current spreading, and device temperature for different contact ratios at a 0.035 mA injection current by simulation.

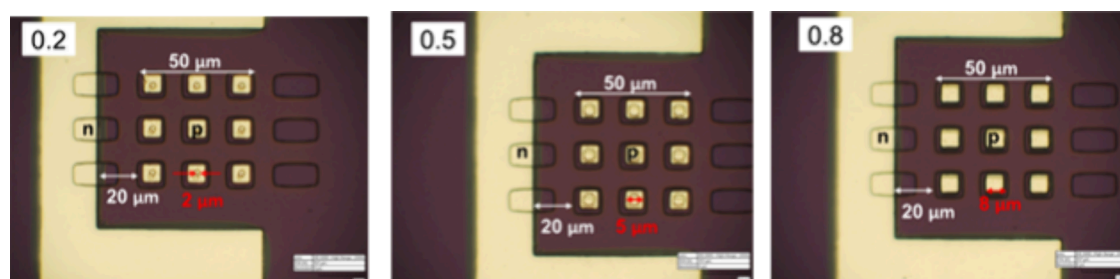


Figure 2. Top-view of 3×3 μ LEDs arrays with 0.2, 0.5, and 0.8 contact ratios.

pattern due to a better current spreading effect. However, it was observed that larger contact sizes also increased the leakage current in the reverse bias region, from 6×10^{-10} to 5.1×10^{-9} A. While this leakage current did not significantly impact the performance of the μ LEDs in this dimension, it becomes a significant factor when the dimension shrinks to $10 \mu\text{m} \times 10 \mu\text{m}$. Therefore, the objective of this study is to investigate the current confinement by adjusting the contact size in $10 \mu\text{m} \times 10 \mu\text{m}$ μ LEDs. We measured and evaluated various optoelectronic characteristics of the μ LEDs, including forward voltage, leakage current, series resistance, parallel resistance, ideality factor, emission output power, emission peak wavelength, full width at half-maximum (FWHM), and external quantum efficiency (EQE). The simulation is discussed in the first part of the study. In addition to analyzing the device performance for different contact ratios, we also examine the current distribution and operating temperature.

EXPERIMENTAL SECTION

To investigate the contact effect in $10 \mu\text{m} \times 10 \mu\text{m}$ μ LEDs, the simulation was carried out in the first part using SpeCLED

software. The contact ratio was varied in three μ LEDs: $2 \mu\text{m} \times 2 \mu\text{m}$, $5 \mu\text{m} \times 5 \mu\text{m}$, and $8 \mu\text{m} \times 8 \mu\text{m}$, named μ LEDA, μ LEDB, and μ LEDC, respectively. The electrical and optical properties were discussed based on the simulation results, including forward voltage, emission output power, wall plug efficiency (WPE), and EQE. The simulation current was set at 0.035 mA, as power chip LEDs are typically examined at 350 mA (at $1000 \mu\text{m} \times 1000 \mu\text{m}$). To observe the current confinement effect and current crowding effect, the lateral current spreading and operating temperatures of the μ LEDs were also analyzed through simulation in this study. The 3D structures of the three contact sizes are shown in Figure 1.

In the experimental part, a commercial 4 in. wafer of InGaN/GaN with a blue LED structure grown on a sapphire substrate was purchased from a vendor and used in this study. A 270 nm-thick ITO layer was first deposited on the wafer as the Ohmic contact layer for the p-GaN layer. The 3×3 arrays with $10 \mu\text{m} \times 10 \mu\text{m}$ pixels were defined using laser direct writing (Heidelberg Instruments, MLA-150) exposure technology. The μ LEDs were manufactured with different contact ratios, as mentioned in the simulation part, requiring the

fabrication of different ITO contact sizes in the first step. After etching the different contact ratios, the mesa process was carried out by using an inductively coupled plasma reactive ion etching (ICP-RIE, Nasca-20 Plus) system. The etching gases used consisted of Cl_2 and BCl_3 at a process pressure of 4 mTorr, resulting in an etching depth of approximately 1 μm into the n-GaN layer. Subsequently, a 500 nm-thick passivation layer of SiO_2 was deposited to cover the sidewall step using plasma-enhanced chemical vapor deposition (PECVD, Samco PD-220N) for each contact ratio. After passivation, the SiO_2 was selectively opened with different contact ratios on each ITO ratio by using an ICP system with SF_6 and O_2 gases. Finally, Ti/Al/Ni/Au multilayer metals were deposited on the ITO and n-GaN as the n- and p-contact electrodes. The top view of each contact ratio is shown in Figure 2. The metal patterns on the p-side for all μLEDs were deposited with an 8 $\mu\text{m} \times 8 \mu\text{m}$ size to act as a mirror. Additionally, the distance between the n- and p-contacts was maintained at 20 μm to prevent shorting during the flip-chip bonding. After the μLEDs process, the current–voltage (I – V) characteristics of the single-chip μLEDs were examined using a semiconductor device analyzer (Keysight, B1500A) through on-wafer measurement at both room temperature and 150 $^\circ\text{C}$.

To measure the emission power from the sapphire side, flip-chip bonding was implemented after μLED fabrication. The μLED arrays were bonded to the circuit on the sapphire substrate by using Ti/Al/Ti/Au metal and an anisotropic conductive film (ACF). Notably, the ACF tape only played the vertical conductivity. Most of the light was reflected by the Ti/Al/Ti/Au metal toward the sapphire side of the μLED device. It is no matter the transparency of ACF. The bonding process was conducted at a temperature of 220 $^\circ\text{C}$ and a pressure of 40 N for 2 min. After the ACF bonding, the μLEDs were packaged in a TO-Can package using wire bonding. This allowed for the diagnosis of the optical properties of the μLEDs using a calibrated integrating sphere, including output power and EQE. The emission pattern was also observed using a CCD and a laser beam profiling instrument (BEAMAGE, Gentec-EO USB 3.0).

RESULT AND DISCUSSION

The electrical-optical properties of the μLED with 10 $\mu\text{m} \times 10 \mu\text{m}$ chip sizes were simulated with different contact ratios using SpeCLED software. Table 1 lists the forward voltage, emission

Table 1. Simulation Data by SpeCLED with the Electrical-Optical Performances of μLEDs

10 $\mu\text{m} \times 10 \mu\text{m}$	0.2	0.5	0.8
input current [mA]		0.035	
forward voltage [V]	2.74	2.60	2.58
output power [μW]	13.3	14.1	14.3
WPE [%]	13.8	15.8	15.9
EQE [%]	12.16	13.24	13.20

output power, WPE, and EQE values at an input current of 0.035 mA (current density of 35 A/cm²). The simulation data show that the voltage decreases from 2.74 to 2.58 V as the contact ratio increases. Moreover, the usage of more MQWs in wider contact ratios results in an increase in output power from 13.3 to 14.3 μW . The μLEDC exhibits a higher WPE value compared to the other samples. Specifically, the WPE of the μLEDC is 2.1% higher than that of the μLEDA , and 0.1%

higher than that of the μLEDB . The similar WPE values between the μLEDB and μLEDC are due to almost identical forward voltage and output power. However, there is a notable trend in EQE values, with the highest EQE exhibited by the μLEDB . This trend can be explained by a higher leakage current in the μLEDC . The current spreading was simulated and is shown in Figure 1. With a higher contact ratio, it is expected that more current will flow into and contact the mesa sidewall, resulting in a higher leakage current and reduced efficiency of the μLEDs . Based on the simulation data, the best optoelectronic performance is achieved by the μLEDB . Additionally, the operating temperature at 0.035 mA for each μLED is also presented in Figure 1. As the contact size increases, the highest temperature decreases from 301.39 to 301.1 $^\circ\text{C}$, with the highest temperature region consistently located in the middle position of the active area. A higher temperature is observed at μLEDA , which is caused by the current crowding effect. The simulation results indicate that a wider contact ratio positively affects better current spreading, thus avoiding the current crowding effect and improving the utilization of MQWs. Therefore, Table 1 shows that the emission output power, WPE, and EQE were significantly enhanced when the contact ratio increased from 0.2 to 0.5. However, the simulation results do not provide information regarding the leakage current, and thus cannot explain the lower EQE observed with a contact ratio of 0.8, which could be attributed to a higher leakage current issue.

As mentioned earlier, in order to validate the simulation results, 10 $\mu\text{m} \times 10 \mu\text{m}$ μLEDs with different contact ratios were fabricated, and the top view of each sample is shown in Figure 2. After the device fabrication process was completed, the electrical characteristics were measured and are shown in Figure 3a. The forward voltage decreases as the contact ratio increases under an injection current of 0.035 mA. Comparing these results with the simulation data, the measured forward voltages were slightly higher: 3.21, 2.77, and 2.74 V for the μLEDA , μLEDB , and μLEDC , respectively. This discrepancy can be attributed to the contact resistance between the p and n electrodes, which is not considered in the simulation and cannot be obtained from SpeCLED software. The series resistance (R_s) and parallel resistance (R_p) were determined by fitting the voltage–current plot using a logarithmic scale. R_p was fitted between 1.4 and 2.4 V before the turn-on voltage of 2.45 V, and then R_s was fitted between 2.4 and 2.6 V. Both R_s and R_p are plotted in Figure 3b. Among the samples, the μLEDA exhibited the highest R_s and lowest R_p , primarily due to its smaller contact size. The schematic of R_s and R_p in the μLED structure is shown in the inset of Figure 3a. Comparing the μLEDA and μLEDC , the R_s value for μLEDA is 0.03 Ω higher than that of μLEDC , while the R_p value for the μLEDA was 0.2 Ω lower than that of μLEDC . The μLEDA exhibits the highest equivalent resistance. The dynamic resistances at 3 V are 158.7, 22.9, and 17.1 k Ω for the μLEDA , μLEDB , and μLEDC , respectively. These results indicate that the dynamic resistance of the μLEDA is 9.3 times higher than that of the μLEDC , which can be attributed to the narrow contact size of only 2 $\mu\text{m} \times 2 \mu\text{m}$. The ideality factors were also calculated from the I – V curve on the logarithmic scale, and they are plotted in Figure 3b using the right axis. Since the turn-on voltage occurred at 2.45 V, the ideal factors were calculated between the forward voltages of 2.4 and 2.6 V. As the contact ratio increases, the ideality factors decrease, with values of 2.38, 1.96, and 1.58 for the μLEDA , μLEDB , and μLEDC ,

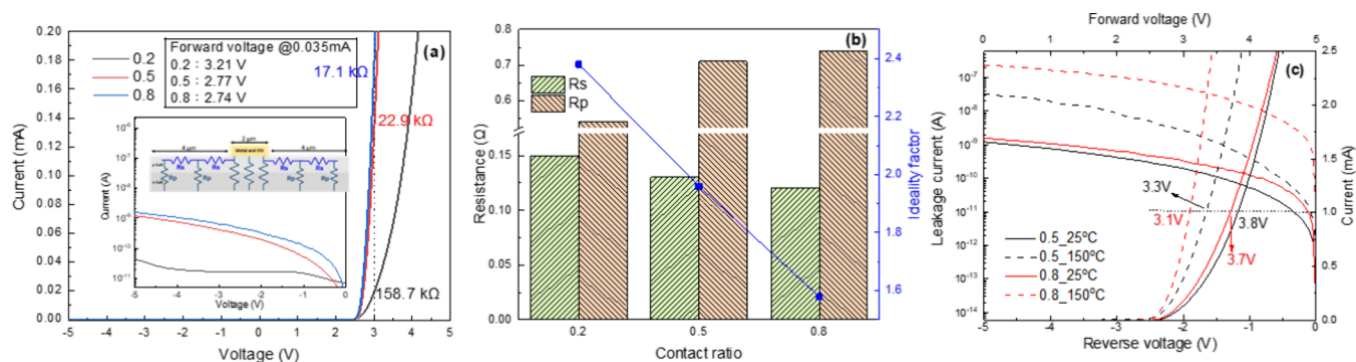


Figure 3. (a) I – V characteristic on-chip measurement, (b) resistance and ideal factor of different contact ratios, and (c) I – V curve of 0.5 and 0.8 contact ratios at 150 °C.

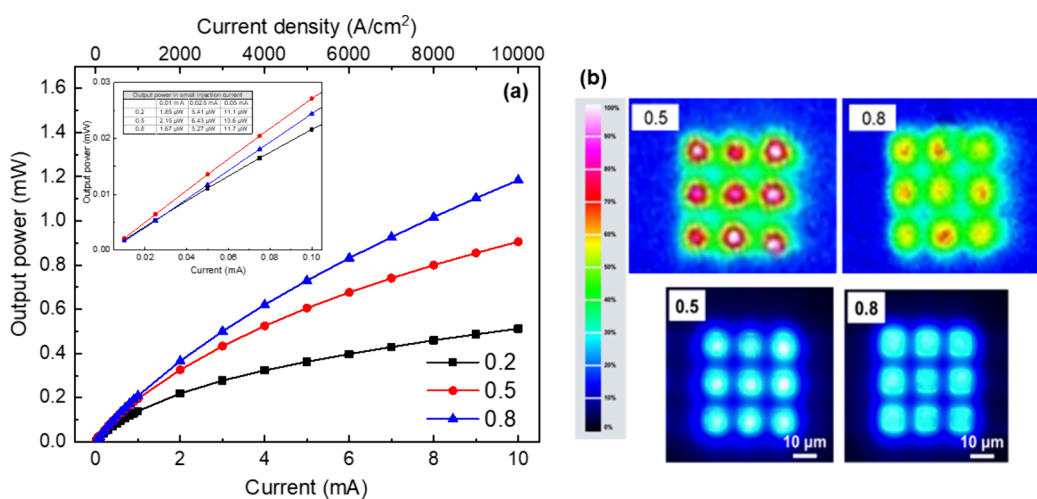


Figure 4. (a) Emission output power of different contact ratios and (b) beam image measurement and emission pattern of 0.5 and 0.8 contact ratios.

respectively. Typically, an ideality factor of 2 indicates that generation and recombination currents dominate and are usually observed at low forward voltages. As the ideality factor exceeds 2, it indicates that the series resistance dominates, especially in GaN power LEDs. In general, the ideality factor value in traditional InGaN-based LEDs always exceeded 2.^{30–33} However, in this study, the μ LEDC exhibited an ideality factor lower than 2 due to perfect current spreading³⁴ and lower contact resistance.

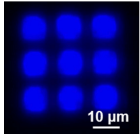
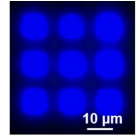
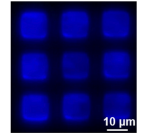
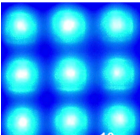
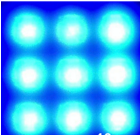
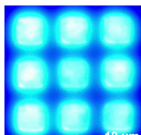
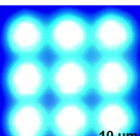
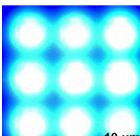
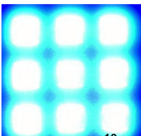
Furthermore, the leakage current in the μ LEDs was measured in reverse voltage and is presented in the inset of Figure 3a. Despite a passivation layer deposited on the devices, the leakage current increased from 44 pA to 1.6 nA as compared with that of μ LEDA and μ LEDC. This indicates that the contact size effectively confines the current and successfully avoids current flowing toward the sidewall, which further reduced the leakage current. To discuss the contact ratios of 0.5 and 0.8, the I – V characteristics were measured at 150 °C and are plotted in Figure 3c. With an increase in the measurement temperature, more energy is supplied to the carriers. At a reverse voltage of -5 V, more carriers were excited from the valence band to the conduction band through defect energy levels. The leakage current of μ LEDC is noticeably higher than that of the μ LEDB. Additionally, the early turn-on phenomenon was more pronounced in the forward voltage of μ LEDC. When the temperature is raised from room temperature to 150 °C, the forward voltages

μ LEDC and μ LEDB shift from 3.7 to 3.1 V and from 3.8 to 3.3 V at 1 mA, respectively. Considering these observations in both forward and reverse voltage, it can be explained that the area of the MQW in the μ LEDC is larger than that in the μ LED with a 0.5 contact ratio. This can be regarded as multiple diodes being paralleled, resulting in a lower voltage for the μ LEDs with higher contact ratios. Due to the distance between the mesa sidewall and contact pad being only 1 μ m, current confinement is ineffective, causing a considerable number of carriers to escape through the shortest sidewall path in the μ LEDC.

The corresponding emission output power and input current were measured and are shown in Figure 4a. As the input current increased from 0.01 to 10 mA, the output power also increased with higher input currents. The μ LEDC with the widest contact ratio (0.8) exhibited a significant enhancement in output power, increasing from 1.66 μ W to 1.19 mW, as shown in Figure 4a. In comparison, the μ LEDs with contact ratios of 0.5 and 0.2 only increased from 2.15 μ W to 0.91 mW and from 1.85 μ W to 0.51 mW, respectively. Clearly, the wider contact ratio showed a steeper slope, indicating better current spreading and lower equivalent resistance. However, when focusing on the performance of the μ LEDs at initial input currents ranging from 0.01 to 0.1 mA (as shown in the inset of Figure 4a), it can be observed that the highest output power occurred in the μ LEDB, followed in the μ LEDA, at injection currents of 0.01 and 0.025 mA. The μ LEDC with the widest

0.8 contact ratio exhibited lower output power than the other two samples in the initial region. However, as the input current increased further, the current crowding effect impacted the performance of μ LEDA, causing the output power of μ LEDC to exceed that of μ LEDA at 0.05 mA. Table 2 presents the

Table 2. Electroluminescent Images of Three Different Contact Sizes

Current (Current density)	10 $\mu\text{m} \times 10 \mu\text{m}$		
	0.2	0.5	0.8
0.003 mA (3 A/cm ²)			
0.05 mA (50 A/cm ²)			
0.1 mA (100 A/cm ²)			

electroluminescent images of the three contact ratios at small injection currents ranging from 0.003 to 0.1 mA. At an injection current of 0.003 mA (corresponding to a current density of 3 A/cm²), the emission intensity of the 0.8 contact ratio was lower than the other two samples. However, as the injection current increased, nonuniform and asymmetric patterns were observed in μ LEDA at 0.05 and 0.1 mA. Meanwhile, based on the emission patterns, the μ LEDB showed better current confinement and spreading, which explains its higher output power compared with that of μ LEDC at small current injection. The emission pictures at an input current of 0.025 mA were also measured using a beam imager and are presented in Figure 4b. Based on the scale bar, it

can be observed that the emission intensity of μ LEDB presented higher than that of μ LEDC at the same integration time. It can be noticed that the current was confined in the middle of the active region in the μ LEDB. This phenomenon is consistent with the simulation results shown in Figure 1. Therefore, as the input current increased from 0.01 to 0.1 mA, the highest output power was observed in the μ LEDB, as shown in the inset of Figure 4a. After that, the output power of the μ LEDC increased more quickly than that of the μ LEDB, as shown in Figure 4a. This can be attributed to the input current injection across the entire active area, resulting in better usage efficiency and current spreading in the μ LEDC sample. At a current of 0.5 mA (corresponding to a current density of 500 A/cm²), the highest current density may introduce the current crowding effect in the μ LEDB, causing the output power of the μ LEDC with the 0.8 contact ratio sample to exceed that of the μ LEDB.

Moreover, it is well-known that the current crowding effect could generate heat in the device, which could significantly impact the performance of μ LEDs, particularly the emission wavelength. To investigate the influence of current crowding on μ LED performance, the emission peak wavelength was measured and is plotted in Figure 5a as the current increased from 0.01 to 10 mA. The figure can be divided into two injection regions: a small injection region from 0.01 to 1 mA and a larger injection region from 1 to 10 mA. Figure 5a demonstrates a blue shift occurring in all samples. However, as the contact ratio decreases, a more pronounced blue shift effect is observed in the small injection region, as shown in the inset of Figure 5a. In this smaller injection region, the wavelengths shifted by 5.80, 5.56, and 4.24 nm for μ LEDA, μ LEDB, and μ LEDC, respectively. The presence of a local electric field in the quantum wells of GaN-based LEDs results in the quantum confined stark effect (QCSE). This local electric field depends on both spontaneous and piezo-electric polarizations existing in InGaN/GaN LEDs.³⁵ Consequently, it causes a blue shift as the current is injected. On the other hand, the presence of current crowding in the device can lead to a red shift in the wavelength due to increasing junction temperature. In the small current injection region, current crowding does not occur. Moreover, in the same small current injection region,

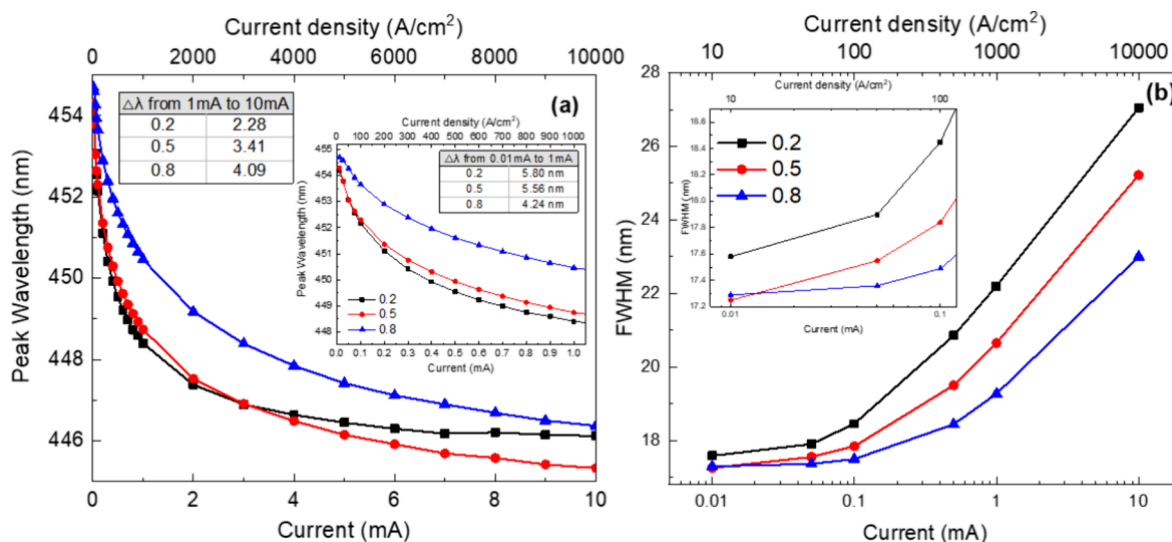


Figure 5. (a) Peak wavelength and (b) FWHM from 10 μA to 10 mA.

μ LEDs with smaller contact ratios experience a larger electric field. This can be demonstrated through simulations and IV characteristics, where a larger external electric field results in a more substantial blue shift. In the higher injection region from 1 to 10 mA, the wavelength shift of μ LEDs was 2.28, 3.41, and 4.09 nm for μ LEDA, μ LEDB, and μ LEDC, respectively. This shift can be attributed to heat generation during high current injection for μ LEDA, which counteracts the blue shift effect and causes a red shift effect. Hence, when the current crowding effect is more pronounced, more heat is generated and the blue shift is offset in the μ LEDA. However, the μ LEDC exhibited better current spreading and no current crowding issues, resulting in the blue shift effect being still evident during the high current injection.

The FWHM of the emission peak was calculated as a function of injection current from 0.01 to 10 mA and is presented in Figure 5b. The inset of this figure shows the small current injection region from 0.01 to 0.1 mA. Based on Figure 5b, it can be observed that the μ LEDA consistently exhibited the widest FWHM in every current injection. This is because the μ LEDA with a smaller contact size restricts current diffusion, resulting in a larger number of carriers filling the MQWs. This effect is known as the “band-filling effect”, which explains why the FWHM is significantly wider in the μ LEDA compared to the other two samples. Furthermore, in the small current density of 10 A/cm², the μ LEDB achieves a narrower FWHM than the μ LEDC. However, as the current density reaches 50 A/cm², the FWHM in the μ LEDA and μ LEDB increases more significantly compared with that in the μ LEDC. This can be attributed to the screen effect, where carriers stack up in the MQWs during higher current density injections. It was suggested that the lower contact resistance and better current spreading effect in the μ LEDC make band filling less pronounced in the MQWs, which also resulted in less screen effect in this contact ratio.

Finally, the EQE values were calculated based on the measured output power using an integrating sphere and are presented in Figure 6. The EQE represents the efficiency of emission output power with respect to the main wavelength and input current. When the input current was increased, the EQE initially increased and then decreased. For the μ LEDs with different contact ratios, the highest EQE values were

obtained at 8.12% (@0.05 mA), 9.95% (@0.075 mA), and 8.93% (@0.1 mA) for the μ LEDA, μ LEDB, and μ LEDC, respectively. The EQE as a function of the initial input current from 0.01 to 0.1 mA is presented in the inset of Figure 6. When the input current is below 0.05 mA, the EQE of the μ LEDC is lower compared to those of the μ LEDA and μ LEDB. However, as the input current is further increased, the current crowding effect starts to significantly decrease the EQE of μ LEDA, as shown in Figure 6. At an input current of 0.4 mA, the μ LEDB and μ LEDC have the EQE values at 8.55 and 8.53%, respectively. Due to superior current spreading and higher efficiency in utilizing MQWs for μ LEDB as compared with those of μ LEDA, and more effective current confinement in μ LEDB than that in μ LEDC, the best EQE was obtained in μ LEDB under low current injection. As the injection current exceeds 0.5 mA, the μ LEDC exhibited a higher EQE value than the μ LEDB. This is because the current crowding effect begins to impact the μ LEDB as the current density reaches 500 A/cm². Additionally, the output power of the μ LEDC exceeds that of the μ LEDB, and the FWHM of the μ LEDB is wider than that of the μ LEDC at 0.5 mA (current density of 500 A/cm²). Consequently, the performance of the μ LEDB becomes degraded. The EQE droop for these μ LEDs is also listed in Figure 6. As the contact ratio increases, the droop values are 38.2, 29.1, and 14.6% for the μ LEDA, μ LEDB, and μ LEDC, respectively. With larger contact sizes, the droop efficiency becomes smaller. The μ LEDC exhibited the least droop. In the case of the μ LEDA, the limited usage of MQWs due to the smallest contact area and the current crowding effect resulted in unsuccessful carrier recombination, leading to the highest droop among the samples with different contact ratios. On the other hand, the μ LEDs with larger contact sizes demonstrate less obvious decay in EQE due to their excellent current spreading and effective utilization of MQWs. Higher injection current results in higher output power and higher EQE values. Therefore, the droop efficiency is lowest for the μ LEDC. However, comparing the EQE decay results between μ LEDA and μ LEDB, it is evident that the μ LEDB exhibited less degradation in EQE. This can be attributed to improved current spreading, lower contact resistance, and effective utilization of MQWs in the design with a 0.5 contact ratio. Overall, the μ LEDB proved to be a good design choice for confining current spreading and achieving outstanding performance in a 10 μ m \times 10 μ m μ LEDs array. The tendency of experimental data aligns well with the simulation results. Nevertheless, the EQE is only influenced by the current spreading effect and MQW usage efficiency using SpecLED simulation. The leakage from the sidewall can not be considered as using the SpecLED. As a result, the lower EQE obtained from the experiment can be attributed to a considerable amount of current flowing directly into the sidewall, as illustrated in Figure 1. This phenomenon resulted in a reduction of carrier recombination behavior in the μ LED device. This is the reason for the EQE discrepancy between simulation and experiment. Based on the traditional power chip definition, the current is always operated at 350 mA (@ 1000 μ m \times 1000 μ m). Under the same current density (35 A/cm²), the μ LED with a 0.5 contact ratio sample demonstrates the best performance with the highest EQE and a better ideality factor of 1.96 in the turn-on voltage region.

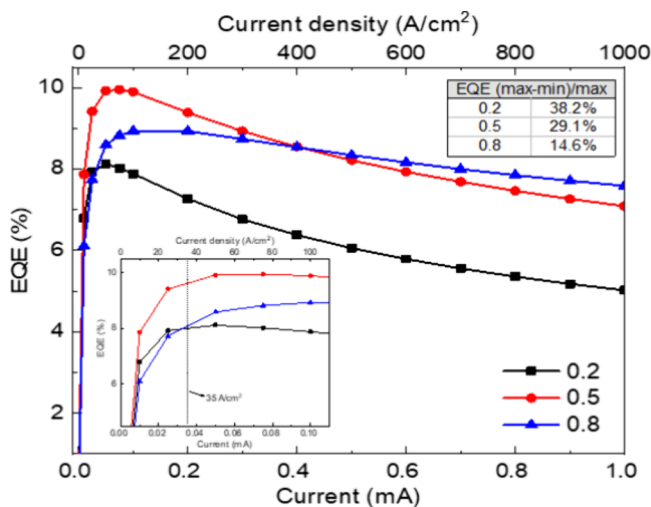


Figure 6. EQE from 10 μ A to 1 mA of different contact ratios.

CONCLUSIONS

In this study, blue light μ LED arrays with different contact ratios and contact sizes (2×2 , 5×5 , and $8 \times 8 \mu\text{m}^2$) were fabricated and simulated. The aim was to investigate the effect of contact size on the performance of the μ LEDs. The simulation results indicated that as the contact ratio increased, the forward voltage decreased from 2.74 to 2.58 V, and the output power increased from 13.3 to 14.3 μW (@0.035 mA). Consequently, the highest EQE of 13.24% was achieved with μ LEDB. The experimental measurements also demonstrated a similar trend in the forward voltage, which was 3.21, 2.77, and 2.74 V (at 0.035 mA) for the different contact ratios. Among the samples, the dynamic resistances of the 0.2 contact ratio were almost 10 times higher than those of the μ LEDC at 3 V. Additionally, an increase in leakage current from 44 pA to 1.6 nA was observed with an increasing contact ratio. As the contact ratio increased, the ideality factors exhibited a droop with values of 2.38, 1.96, and 1.58, respectively. When comparing the output power with different contact ratios and focusing on the input current range of 0.01–0.1 mA, the highest output power was obtained with the μ LEDB. In the initial region, the μ LEDC with a wider 0.8 contact ratio exhibited lower output power compared to the other two samples. However, as the input current further increased, the current crowding effect began to impact the performance of the μ LEDA and the output power of the μ LEDC exceeded that of the μ LEDA at 0.05 mA. The emission peak wavelength confirmed this phenomenon as the red shift effect was more prominent in the μ LEDA, which inhibited the blue shift effect in the high injection region. The FWHM plot indicated that the narrowest FWHM was exhibited by the 0.5 contact ratio at an injection current of 0.01 mA (current density of 10 A/cm²). However, as the injection current increased, the FWHM of the μ LEDB broadened due to the screen effect. Finally, the highest EQE of 9.95% was achieved with the μ LEDB. Based on these findings, it is recommended to use a contact ratio of 0.5 in 10 $\mu\text{m} \times 10 \mu\text{m}$ μ LEDs, as this contact size successfully confines the current and better current spreading, which leads to improved performance.

AUTHOR INFORMATION

Corresponding Author

Ray-Hua Horng – Institute of Electronics, National Yang Ming Chiao Tung University, Hsinchu 30010, Taiwan, ROC; orcid.org/0000-0002-1160-6775; Email: rayhua@nycu.edu.tw

Authors

Yu-Hsuan Hsu – Department of Photonics, College of Electrical and Computer Engineering, National Yang Ming Chiao Tung University, Hsinchu 30010, Taiwan, ROC

Yi-Hsin Lin – Department of Photonics, College of Electrical and Computer Engineering, National Yang Ming Chiao Tung University, Hsinchu 30010, Taiwan, ROC

Ming-Hsien Wu – Electronic and Optoelectronic System Research Laboratories, Industrial Technology Research Institute, Hsinchu 310401, Taiwan, ROC

Hao Chung Kuo – Department of Photonics, College of Electrical and Computer Engineering, National Yang Ming Chiao Tung University, Hsinchu 30010, Taiwan, ROC

Complete contact information is available at:

<https://pubs.acs.org/10.1021/acsomega.3c05265>

Funding

This study was supported by the National Science and Technology Council (NSTC), Taiwan, ROC, under the grants NSTC 111-2218-E-A49-019-MBK and 112-2218-E-A49-022-MBK. This study was also supported by the Science Park Emerging Technology Application Program, Taiwan, ROC, under the grant 111AO29B and B11202.

Notes

The authors declare no competing financial interest.

ACKNOWLEDGMENTS

We thank the Nano Facility Center at National Yang Ming Chiao Tung University, Taiwan Semiconductor Institute Research, MA-tek and Taiwan Instrument Research Institute for their facilities support.

REFERENCES

- (1) Wierer, J.; Tansu, N. III-Nitride Micro-LEDs for Efficient Emissive Displays. *Laser Photonics Rev.* **2019**, *13*, No. 1900141.
- (2) Wong, M. S.; Nakamura, S.; DenBaars, S. P. Review-Progress in High Performance III-Nitride Micro-Light-Emitting Diodes. *ECS J. Solid State Sci. Technol.* **2019**, *9*, No. 015012.
- (3) Weisbuch, C. Review-On The Search for Efficient Solid State Light Emitters: Past, Present, Future. *ECS J. Solid State Sci. Technol.* **2020**, *9* (1), No. 016022.
- (4) Zhang, Y.; Xu, R.; Kang, Q.; Zhang, X.; Zhang, Z. H. Recent Advances on GaN-Based Micro-LEDs. *Micromachines* **2023**, *14* (5), 991.
- (5) Wu, Y. F.; Ma, J. S.; Su, P.; Zhang, L. J.; Xia, B. Z. Full-Color Realization of Micro-LED Displays. *Nanomaterials* **2020**, *10* (12), 2482.
- (6) Zhu, G. Q.; Liu, Y. J.; Ming, R.; Shi, F.; Cheng, M. J. Mass transfer, detection and repair technologies in micro-LED displays. *Sci. China-Mater.* **2022**, *65* (8), 2128–2153.
- (7) Gong, Y.; Gong, Z. Laser-Based Micro/Nano-Processing Techniques for Microscale LEDs and Full-Color Displays. *Adv. Mater. Technol.* **2023**, *8* (5), No. 2200949.
- (8) Anwar, A. R.; Sajjad, M. T.; Johar, M. A.; Hernández-Gutiérrez, C. A.; Usman, M.; Łepkowski, S. P. Recent Progress in Micro-LED-Based Display Technologies. *Laser Photon. Rev.* **2022**, *16* (6), No. 2100427.
- (9) Chen, F. R.; Bian, J.; Hu, J. L.; Sun, N. N.; Yang, B.; Ling, H.; Yu, H. Y.; Wang, K. X.; Gai, M. X.; Ma, Y. H.; Huang, Y. A. Mass transfer techniques for large-scale and high-density microLED arrays. *Int. J. Extreme Manuf.* **2022**, *4* (4), No. 042005.
- (10) Kim, H. M.; Ryu, M.; James, H. J.; Cha, H. S.; Kim, T. Jeong; Jang, J. Ten micrometer pixel, quantum dots color conversion layer for high resolution and full color active matrix micro-LED display. *J. Soc. Inf. Display* **2019**, *27* (6), 347–353.
- (11) Yang, J.; Choi, M. K.; Yang, U. J.; Kim, S. Y.; Kim, Y. S.; Kim, J. H.; Kim, D. H.; Hyeon, T. Toward Full-Color Electroluminescent Quantum Dot Displays. *Nano Lett.* **2021**, *21* (1), 26–33.
- (12) Zhao, J.; Chen, L. X.; Li, D. Z.; Shi, Z. Q.; Liu, P.; Yao, Z. L.; Yang, H. C.; Zou, T. Y.; Zhao, B.; Zhang, X.; Zhou, H.; Yang, Y. X.; Cao, W. R.; Yan, X. L.; Zhang, S. D.; Sun, X. W. Large-area patterning of full-color quantum dot arrays beyond 1000 pixels per inch by selective electrophoretic deposition. *Nat. Commun.* **2021**, *12* (1), 4603.
- (13) Mei, W. H.; Zhang, Z. Q.; Zhang, A. D.; Li, D.; Zhang, X. Y.; Wang, H. W.; Chen, Z.; Li, Y. Z.; Li, X. G.; Xu, X. G. High-resolution, full-color quantum dot light-emitting diode display fabricated via photolithography approach. *Nano Res.* **2020**, *13* (9), 2485–2491.
- (14) Zhao, B. X.; Wang, Q. Q.; Li, D. P.; Yang, H. C.; Bai, X.; Li, S.; Liu, P.; Sun, X. W. Red and Green Quantum Dot Color Filter for Full-Color Micro-LED Arrays. *Micromachines* **2022**, *13* (4), 595.
- (15) Li, P. Y.; Tao, J.; Zhao, Y. Z.; Sun, Y. F.; Fan, K. L.; Zhu, L. C.; Sun, W. C.; Lv, J. G.; Qin, Y. X.; Wang, Q. Flexible Quantum-Dot

Color-Conversion Layer Based on Microfluidics for Full-Color Micro-LEDs. *Micromachines* **2022**, *13* (3), 448.

(16) Huang, Y. M.; Chen, J. H.; Liou, Y. H.; Singh, K. J.; Tsai, W. C.; Han, J.; Lin, C. J.; Kao, T. S.; Lin, C. C.; Chen, S. C.; Kuo, H. C. High-Uniform and High-Efficient Color Conversion Nanoporous GaN-Based Micro-LED Display with Embedded Quantum Dots. *Nanomaterials* **2021**, *11* (10), 2696.

(17) Yang, H. S.; Han, S. Y.; Hlad, M.; Gila, B. P.; Baik, K. H.; Pearton, S. J.; Jang, S.; Kang, B. S.; Ren, F. Comparison of Surface Passivation Layers on InGaNGaN MQW LEDs. *J. Semicond. Technol. Sci.* **2005**, *5* (2), 131–135.

(18) Liu, Y. H.; Hsu, W. C.; Chou, B. Y.; Wang, Y. H.; Sun, W. C.; Wei, S. Y.; Yu, S. M. Al₂O₃ Passivation Layer for InGaN/GaN LED Deposited by Ultrasonic Spray Pyrolysis. *IEEE Photonics Technol. Lett.* **2014**, *26* (12), 1243–1246.

(19) Chen, D. B.; Wang, Z.; Hu, F. C.; Shen, C.; Chi, N.; Liu, W. J.; Zhang, D. W.; Lu, H. L. Improved electro-optical and photoelectric performance of GaN-based micro-LEDs with an atomic layer deposited AlN passivation layer. *Opt. Express* **2021**, *29* (22), 36559–36566.

(20) Wang, Y. L.; Kim, H. S.; Norton, D. P.; Pearton, S. J.; Ren, F. Dielectric passivation effects on ZnO light emitting diodes. *Appl. Phys. Lett.* **2008**, *92* (11), 112101.

(21) Wong, M. S.; Hwang, D.; Alhassan, A. I.; Lee, C.; Ley, R.; Nakamura, S.; Denbaars, S. P. High efficiency of III-nitride micro-light-emitting diodes by sidewall passivation using atomic layer deposition. *Opt. Express* **2018**, *26* (16), 21324–21331.

(22) Lee, H.; Lee, J. H.; Park, J. S.; Seong, T. Y.; Amano, H. Improving the Leakage Characteristics and Efficiency of GaN-based Micro-Light-Emitting Diode with Optimized Passivation. *ECS J. Solid State Sci. Technol.* **2020**, *9* (5), No. 005001.

(23) Yeh, Y. W.; Lin, S. H.; SH, T. C.; Hsu, S. Q.; Lai, P. T.; Lee, S. Y.; Lien, D. S.; Wu, G. S.; Li, Z.; Chen, T. Z.; Wu, H. C.; Kuo. Advanced Atomic Layer Deposition Technologies for Micro-LEDs and VCSELs. *Nanoscale Res. Lett.* **2021**, *16* (1), 164.

(24) Lee, T. Y.; Huang, Y. M.; Chiang, H.; Chao, C. L.; Hung, C. Y.; Kuo, W. H.; Fang, Y. H.; Chu, M. T.; Wu, C. I.; Lin, C. C.; Kuo, H. C. Increase in the efficiency of III-nitride micro LEDs by atomic layer deposition. *Opt. Express* **2022**, *30* (11), 18552–18561.

(25) Zhuang, D.; Edgar, J. H. Wet etching of GaN, AlN, and SiC: a review. *Mater. Sci. Eng. R-Rep.* **2005**, *48* (1), 1–46.

(26) Wan, H.; Tang, B.; Li, N.; Zhou, S. J.; Gui, C. Q.; Liu, S. Revealing the Role of Sidewall Orientation in Wet Chemical Etching of GaN-Based Ultraviolet Light-Emitting Diodes. *Nanomaterials* **2019**, *9* (3), 365.

(27) Yu, J. C.; Tao, T.; Liu, B.; Xu, F. F.; Zheng, Y.; Wang, X.; Sang, Y. M.; Yan, Y.; Xie, Z. L.; Liang, S. H.; Chen, D. J.; Chen, P.; Xiu, X. Q.; Zheng, Y. D.; Zhang, R. Investigations of Sidewall Passivation Technology on the Optical Performance for Smaller Size GaN-Based Micro-LEDs. *Crystals* **2021**, *11* (4), 403.

(28) Wong, M. S.; Lee, C.; Myers, D. J.; Hwang, D.; Kearns, J. A.; Li, T.; Speck, J. S.; Nakamura, S.; DenBaars, S. P. Size-independent peak efficiency of III-nitride micro-light-emitting-diodes using chemical treatment and sidewall passivation. *Appl. Phys. Express* **2019**, *12* (9), No. 097004.

(29) Hsu, Y. H.; Lo, Y. Y.; Lin, Y. H.; Zan, H. W.; Horng, R. H. Effects of ITO Contact Sizes on Performance of Blue Light MicroLEDs. *Nanoscale Res. Lett.* **2022**, *17* (1), 113.

(30) Dalapati, P.; Manik, N. B.; Basu, A. N. Analysis of the Temperature Dependence of Diode Ideality Factor in InGaN-Based UV-A Light-Emitting Diode. *Semiconductors* **2020**, *54* (10), 1284–1289.

(31) Zhu, D.; Xu, J. R.; Noemaun, A. N.; Kim, J. K.; Schubert, E. F.; Crawford, M. H.; Koleske, D. D. The origin of the high diode-ideality factors in GaInN/GaN multiple quantum well light-emitting diodes. *Appl. Phys. Lett.* **2009**, *94* (8), No. 081113.

(32) Casey, H. C.; Muth, J.; Krishnankutty, S.; Zavada, J. Dominance of tunneling current and band filling in InGaN/AlGaIn

double heterostructure blue light-emitting diodes. *Appl. Phys. Lett.* **1996**, *68* (20), 2867–2869.

(33) Chitnis, A.; Kumar, A.; Shatalov, M.; Adivarahan, V.; Lunev, A.; Yang, J. W.; Simin, G.; Khan, M. A.; Gaska, R.; Shur, M. High-quality p–n junctions with quaternary AlInGaN/InGaN quantum wells. *Appl. Phys. Lett.* **2000**, *77* (23), 3800–3802.

(34) Huang, S. J.; Fan, B. F.; Chen, Z. M.; Zheng, Z. Y.; Luo, H. T.; Wu, Z. S.; Wang, G.; Jiang, H. Lateral Current Spreading Effect on the Efficiency Droop in GaN Based Light-Emitting Diodes. *J. Dispersion Technol.* **2013**, *9* (4), 266–271.

(35) Fiorentini, V.; Bernardini, F.; Della Sala, F.; Di Carlo, A.; Lugli, P. Effects of macroscopic polarization in IIIV nitride multiple quantum wells. *Phys. Rev. B* **1999**, *60* (12), 8849–8858.